Cell PRESS
Structure
Article

Transducer Binding Establishes Localized Interactions to Tune Sensory Rhodopsin II

David A. Cisneros,[1,4] Leoni Oberbarnscheidt,[2] Angela Pannier,[1] Johann P. Klare,[3,5] Jonne Helenius,[1] Martin Engelhard,[3] Filipp Oesterhelt,[2,*] and Daniel J. Muller[1,*]
[1]Biotechnology Center, University of Technology, Dresden, Germany
[2]Physikalische Chemie II, Heinrich-Heine-Universität, Düsseldorf, Germany
[3]Max-Planck-Institute for Molecular Physiology, Dortmund, Germany
[4]Present address: Molecular Genetics Unit and CNRS URA2172, Institut Pasteur, Paris, France
[5]Present address: Fachbereich Physik, Universität Osnabrück, Germany
*Correspondence: filipp.oesterhelt@uni-duesseldorf.de (F.O.), mueller@biotec.tu-dresden.de (D.J.M.)
DOI 10.1016/j.str.2008.04.014

SUMMARY

In haloarchaea, sensory rhodopsin II (SRII) mediates a photophobic response to avoid photo-oxidative damage in bright light. Upon light activation the receptor undergoes a conformational change that activates a tightly bound transducer molecule (HtrII), which in turn by a chain of homologous reactions transmits the signal to the chemotactic eubacterial two-component system. Here, using single-molecule force spectroscopy, we localize and quantify changes to the intramolecular interactions within SRII of *Natronomonas pharaonis* (NpSRII) upon NpHtrII binding. Transducer binding affected the interactions at transmembrane α helices F and G of NpSRII to which the transducer was in contact. Remarkably, the interactions were distributed asymmetrically and significantly stabilized α helix G entirely but α helix F only at its extracellular tip. These findings provide unique insights into molecular mechanisms that "prime" the complex for signaling, and guide the receptor toward transmitting light-activated structural changes to its cognate transducer.

INTRODUCTION

Microbial rhodopsins absorb light energy for ion transport or photosensation (Sharma et al., 2006). These photoreceptors are membrane proteins that share a common structural motif consisting of seven transmembrane α helices, A–G. A Schiff base located at the middle of the seventh α helix G covalently links the all-*trans* retinal chromophore to the protein. In haloarchaea, four different classes of microbial rhodopsins have been identified. Two of these, bacteriorhodopsin and halorhodopsin, use light to transport ions across the membrane and to establish ion gradients used as an energy source by other proteins. The other two retinal proteins, sensory rhodopsin I (SRI) and sensory rhodopsin II (SRII), mediate phototactic and photophobic responses, respectively. In addition, SRI mediates a repellent response after being activated by two sequential photons (Spudich and Bogomolni, 1984). SRI and SRII bind tightly to their cognate transducers, HtrI and HtrII, which upon activation by the receptor elicit a response via a cascade homologous to the chemotactic eubacterial two-component system. Both transducers contain two transmembrane α helices (TM1 and TM2) and a large cytoplasmic domain. Whereas the transmembrane domains of the transducer bind to the receptor and receive the light-activated signal, the two cytoplasmic subdomains transfer this signal to histidine kinase (CheA) (for reviews, see Klare et al., 2004, 2008; Spudich, 2006).

A model describing how the signal is transferred from SRII to its cognate transducer (HtrII) was proposed based on biochemical (Bergo et al., 2003; Wegener et al., 2000) and structural (Luecke et al., 2001; Wegener et al., 2001; Gordeliy et al., 2002; Moukhametzianov et al., 2006) data. Light excitation leads to the isomerization of the retinal chromophore from the all-*trans* to the 13-*cis* conformation, which due to thermal relaxation is followed by conformational changes in SRII. The protein passes through a series of spectroscopically detectable intermediates (Chizhov et al., 1998) denoted K, L, M, N, and O (named after BR intermediates). A spectroscopically silent irreversible reaction occurs between two M-states, M_1 and M_2, which has been correlated with the signaling state (Chizhov et al., 1998). In vivo experiments support this conclusion (Yan et al., 1991). Likely, signal transfer occurs when α helices F and G in SRII change conformations. These tilt and rotate the cytoplasmic side of the transmembrane α helix 2 of the bound HtrII (Moukhametzianov et al., 2006; Spudich, 2006).

In this study, we used single-molecule force spectroscopy (SMFS) to measure the interactions of SRII in the absence and in the presence of its transducer, HtrII (for a review on this technique, see Kedrov et al., 2007). SRII from *Natronomonas pharaonis* (NpSRII) was chosen because it represents the best characterized haloarchaeal photophobic rhodopsin receptor (Gordeliy et al., 2002; Klare et al., 2008; Spudich, 2006). Single-molecule force-distance (F-D) spectra for the mechanical unfolding of NpSRII and of NpSRII + NpHtrII complexes reconstituted in purple membrane lipids were obtained. The unfolding pattern, reflecting the interactions that stabilize structures within the receptors, was similar to that obtained previously of other archaeal rhodopsins (Cisneros et al., 2005; Muller et al., 2002). Introducing a simple method to analyze the membrane protein unfolding spectra, we could structurally map the interactions that have been established within the average NpSRII molecule. This

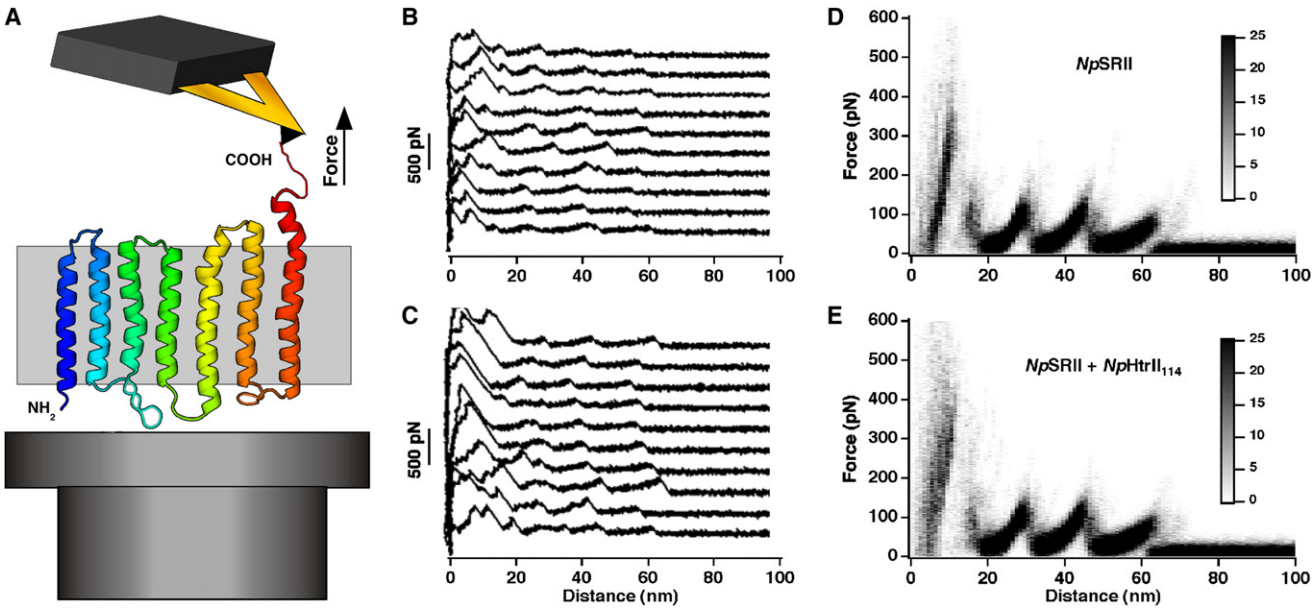

Figure 1. SMFS of NpSRII Alone and of NpSRII in a Complex with NpHtrII$_{114}$

(A) Contacting the terminal end of a single NpSRII with a molecularly sharp AFM tip forces the attachment of both. This molecular link allows exertion of a mechanical pulling force that initiates the stepwise unfolding of the receptor (here shown without transducer). (B) F-D curves recorded while unfolding single NpSRII molecules and (C) in complex with NpHtrII$_{114}$ by pulling from the C-terminal end. Superimpositions of F-D curves recorded from unfolding of (D) NpSRII alone and (E) NpSRII + NpHtrII$_{114}$ complexes. Superimpositions are represented as a density plots. F-D curves were obtained at room temperature at a pulling speed of ~300 nm/s in buffer solution (pH 7.8, Tris-HCl 20 mM, 300 mM KCl).

approach allows single-molecule experiments to describe the interactions common to all NpSRII molecules, normally revealed by conventional bulk experiments. The comparison of structural interaction maps revealed from SMFS disclosed the interactions of NpSRII that changed upon NpHtrII binding. Detectable changes were restricted to α helices F and G. Functional consequences are discussed in detail.

RESULTS

SMFS of NpSRII with and without Bound Transducer

To determine the interactions that stabilize structural regions of NpSRII and NpSRII bound to a truncated form of its transducer (NpHtrII$_{114}$), we applied SMFS as previously established for other archaeal rhodopsins and membrane proteins (Kedrov et al., 2007). Briefly, NpSRII and NpSRII bound to NpHtrII$_{114}$ were reconstituted in purple membrane lipids (Wegener et al., 2001). Subsequently, each sample was adsorbed to freshly cleaved mica supports (Muller et al., 1997). Resulting membrane patches were imaged using AFM (data not shown) and selected for SMFS analysis. After switching the AFM to the SMFS mode, single NpSRII molecules in the absence (NpSRII) or presence of their transducer (NpSRII + NpHtrII$_{114}$ complex) were attached nonspecifically to the AFM tip (Figure 1A; Oesterhelt et al., 2000). Retracting the AFM tip from the membrane induced the unfolding of single NpSRIIs. F-D curves recorded showed characteristic patterns of unfolding events (Cisneros et al., 2005; Muller et al., 2002). F-D curves of single NpSRII molecules attached by their C-terminal end to the AFM tip (see Experimental Procedures) were selected for further analysis. A total of 164 F-D curves were collected for NpSRII alone and 125 for the NpSRII + NpHtrII$_{114}$ complex. Every peak of an F-D curve represented the unfolding of one stable segment of the membrane protein (Janovjak et al., 2006; Kedrov et al., 2007). At first glance, the F-D curves tracing the unfolding process of NpSRII (Figure 1B) and NpSRII in presence of NpHtrII$_{114}$ (Figure 1C) were similar. However, individual F-D traces differed slightly from each other, lacking some force peaks or presenting force peaks at slightly different positions or of different strengths. To observe common features, the F-D traces were superimposed and displayed as density plots (Figures 1D and 1E). Such superimpositions represent the average F-D spectrum recorded. The superimpositions highlighted the same five major force peaks recorded for NpSRII alone (Figure 1D) and the NpSRII + NpHtrII$_{114}$ complex (Figure 1E). Comparing single F-D curves and the superimposed spectrum for the NpSRII alone (Figures 1B and 1D) with those for the NpSRII + NpHtrII$_{114}$ complex (Figures 1C and 1E) revealed differences within the first 20 nm of pulling. In this region the NpSRII + NpHtrII$_{114}$ complex showed larger forces and a higher density of force peaks.

Mapping the Probability at Which Force Peaks Occurred

While SMFS unfolding of bovine rhodopsin (Sapra et al., 2006b), bacteriorhodopsin (Muller et al., 2002), and halorhodopsin (Cisneros et al., 2005), we observed that each force peak within a F-D curve had a certain probability of occurring. To quantify the differences in peak appearance probability between F-D curves obtained from NpSRII alone and from the NpSRII + NpHtrII$_{114}$ complex, we fitted each force peak detected in individual F-D curves using the WLC model. As derived from the WLC fit, we

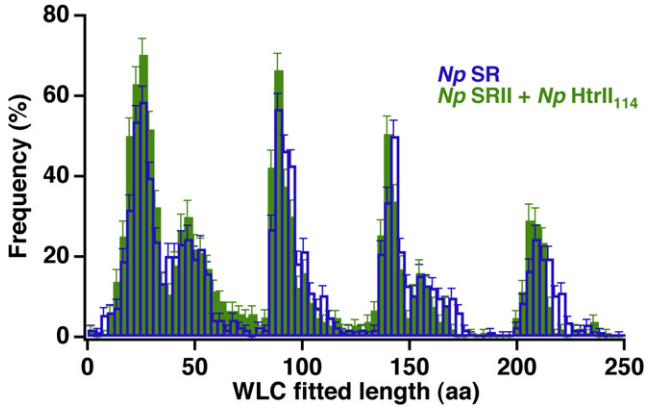

Figure 2. Frequency of Force Peaks Detected at Different Portions of the Stretched Polypeptide

Every force peak detected in individual F-D curves (Figure 1) was fitted using the WLC model, using the contour length of the polypeptide (L) as the only fitting parameter. The frequency at which the force peaks occurred is plotted in a histogram. NpSRII (blue, n = 164) and NpSRII + NpHtrII$_{114}$ complex (green, n = 125). Error bars represent the standard error of the mean (SEM). The length of the polypeptide is given in amino acids (aa). The bin size of the histogram is 3 aa and corresponds to the average precision at which individual force peaks could be fitted using the WLC model (Bustamante et al., 1994).

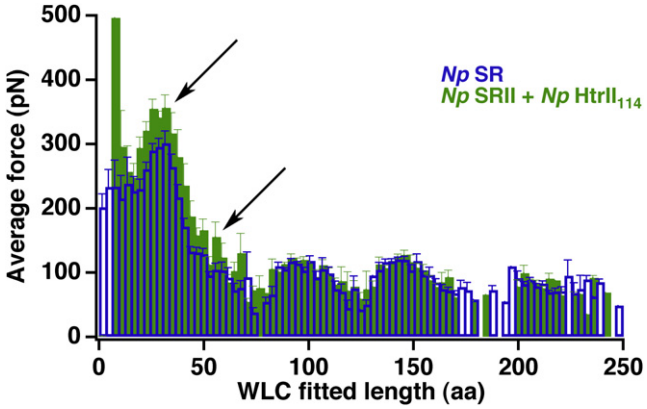

Figure 3. Average Force Detected at Different Positions of the Stretched Polypeptide

The force of every peak detected in an F-D curve was measured. The average force of force peaks are plotted at the WLC fitted lengths at which they were detected. Error bars represent the SEM. For each length of the stretched polypeptide, force peaks detected within 3 aa were pooled and averaged. Blue bars represent the average forces detected for NpSRII alone, the green bars the average forces detected for the NpSRII + NpHtrII$_{114}$ complex. Arrows indicate large changes in the interaction forces (see text for details).

converted the peak position measured in nanometers into the amino acid length of the stretched portion of the polypeptide (Muller et al., 2002; Oesterhelt et al., 2000). The frequency at which each force peak was detected at a certain position was plotted over the length of the stretched polypeptide (Figure 2). The findings showed a remarkable similarity of the occurrence of interactions detected between NpSRII alone (Figure 2, blue bars) and of NpSRII in complex with NpHtrII$_{114}$ (Figure 2, green bars). However, small differences were observed. These differences were distributed over most of the polypeptide lengths ranging from 15–25 aa, 60–80 aa, 140–170 aa, and 210–240 aa.

Determining the Average Interaction Strength of Force Peaks

Interactions within bacteriorhodopsin and other rhodopsins depend on boundary conditions such as pH, electrolyte (Kessler and Gaub, 2006; Park et al., 2007), temperature (Janovjak et al., 2003), point mutations (Sapra et al., 2008), and the oligomeric assembly (Sapra et al., 2006a). To quantify the interaction forces that changed within NpSRII upon formation of the NpSRII + NpHtrII$_{114}$ complex, we measured the strength of each force peak detected in the absence and in the presence of the transducer. The forces of all peaks occurring within a window of 3 aa were averaged and plotted over the stretched polypeptide length (Figure 3). Unlike the histogram of peak appearance frequency (Figure 2), the average forces plotted over the polypeptide length showed some pronounced changes occurring within the first 80 aa (Figure 3). At higher polypeptide lengths, the average forces were not significantly different. Within the first 50 aa of the polypeptide, the NpSRII + NpHtrII$_{114}$ complexes (Figure 3, blue bars) displayed higher forces compared with the NpSRII characterized in absence of the transducer (Figure 3, green bars).

Normalizing the Average Interaction Strengths of NpSRII

As calculated, the average peak force does not fully represent the interaction strength of a given structure. This is because the average force (Figure 3) did not take into account interactions (peaks) too weak to be detected. To normalize the average force, we multiplied the probability at which a force peak occurred (Figure 2) by the average force of the peak (Figure 3). The normalized average force reflects the average interaction strength established within a randomly picked NpSRII molecule. Or, seen from the bulk behavior, the normalized average force corresponds to that of all NpSRII molecules. Displaying the normalized average forces over the polypeptide length of NpSRII (Figure 4A) enhanced the differences in the interaction strengths between NpSRII with and without NpHtrII$_{114}$ bound. The distribution of these structural changes is highlighted when the differences between the normalized interactions strengths for each of the NpSRII molecule states is plotted (Figure 4B). In Figure 4A, the SEM shown in Figures 2 and 3 were used to calculate the SEM according to the following formula: $(SEM_{FP}/(F \cdot P))^2 = (SEM_{force}/F)^2 + (SEM_{prob}/P)^2$, where F is the mean force (Figure 2) and P is the probability (Figure 3) of a peak. For Figure 4B, the SEM was calculated as $SEM_{\Delta FP}{}^2 = SEM_{FP2}{}^2 + SEM_{FP1}{}^2$, where SEM_{FP2} and SEM_{FP1} are the normalized forces, F·N, calculated in Figure 4A for NpSRII bound or unbound to NpHtrII.

Mapping the Normalized Interactions onto the NpSRII Sequence

A force peak detected in the F-D spectrum denotes an interaction detected at a certain distance from the AFM tip (Kedrov et al., 2007). This distance is the length of the stretched polypeptide and can be used to locate the structural region of the membrane protein at which an interaction established a sufficient strength to be detected by SFMS. However, to correctly locate the interactions detected upon unfolding of NpSRII, it must be considered that some of the interactions establishing the

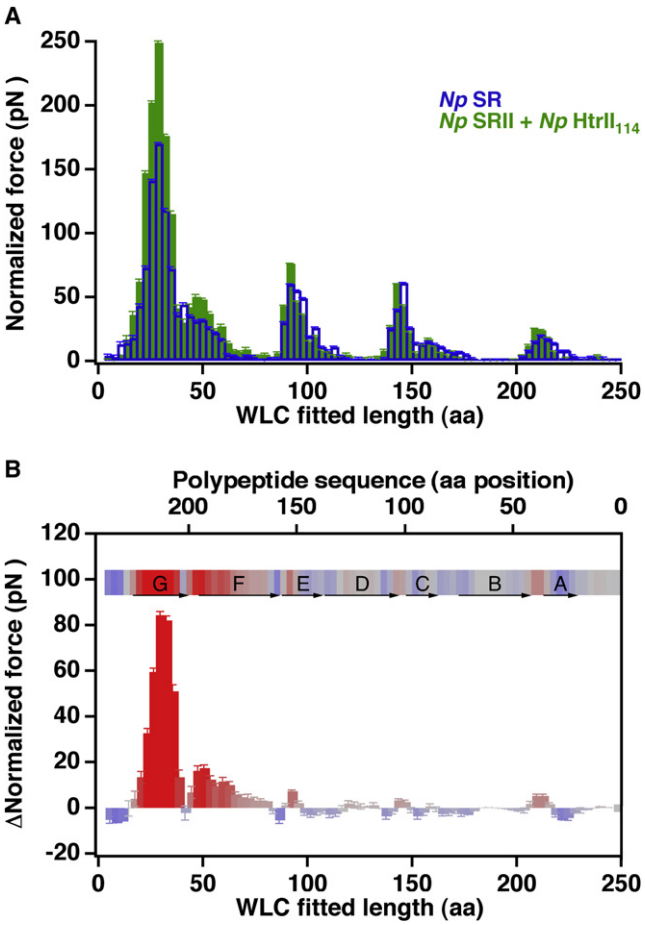

Figure 4. Normalizing and Mapping the Interactions Established within NpSRII upon Binding the Transducer (NpHtrII$_{114}$)

To combine force and probability (Figure 1), the average force (Figure 3) was multiplied with the frequency of force-peak appearance (Figure 2). (A) Normalized forces measured for NpSRII alone (blue) and for NpSRII complexed with NpHtrII$_{114}$ (green) are plotted. Error bars represent SEM. (B) Difference calculated between normalized interaction strengths detected for NpSRII without and with transducer (A) shows the interactions established upon NpHtrII$_{114}$ binding to NpSRII. The color scale (inset bar, saturated at 20 pN) indicates changes of the normalized force (positive = red, negative = blue). The bar above the force difference histogram (B) maps the interaction differences onto the loops and helices (lettered A–G) of the NpSRII structure. The lower x axis of the histogram shows the length of the stretched polypeptide as revealed from WLC fitting individual force peaks in the F-D spectra. The upper x axis reflects the amino acid position of structures holding the stretched NpSRII polypeptide chain. Small shifts in the positions of the force differences mapped onto the length of the stretched polypeptide (lower x axis) and onto the NpSRII polypeptide (upper x axis and scale bar above histogram) occur because systematic errors in the position of structural interactions lying within the membranes are corrected (see Experimental Procedures).

anchoring points of the polypeptide were located inside the membrane (Muller et al., 2002). Because the pulling distance is referred to the membrane surface, the position of unfolding barriers located inside the membrane had to be corrected. Thus, each polypeptide region at which the interaction occurred was located (Figure 4B). This correlation, shown in Figure 4B, highlights major differences in interactions detected within the first 70 C-terminal amino acids of NpSRII. Notably, the other NpSRII structures showed only minor variations (>70 aa; Figure 4B). The highest force difference of ~80 pN (Figure 4B) was centered at amino acid 34 of the stretched polypeptide, which corresponds to amino acid position ~211 (α helix G) as counted from the N-terminal end. A second maximum of ~18 pN was observed at a stretched polypeptide length of ~45 aa, or approximately amino acid position 174 (α helix F).

DISCUSSION

In recent years, SMFS has been applied to elucidate the unfolding pathways of bacteriorhodopsin (Muller et al., 2002), halorhodopsin (Cisneros et al., 2005), proteorhodopsin (Klyszejko et al., 2008), bovine rhodopsin (Sapra et al., 2006b), and several other membrane proteins (Kedrov et al., 2004, 2007). As expected, the unfolding pattern of NpSRII (Figures 1D and 1E) is similar to those observed of other archaeal rhodopsins, and different to that of bovine rhodospin. In bovine rhodopsin, the tendency of individual structural segments to unfold together in cooperative events is much more pronounced (Sapra et al., 2006b). In addition, the interactions detected by SMFS and mapped onto rhodopsin show less correlation to the secondary structures. Differences in the unfolding behavior may indicate that these proteins are nonhomologous (Sharma et al., 2006). However, the similarity of unfolding patterns of different archeal rhodopsins indicate that they are not only structurally and functionally similar (Sharma et al., 2006) but also that their intramolecular interactions have been conserved.

Applying a New Procedure to Analyze F-D Spectra

In previous work, we have introduced the superimposition of F-D curves to highlight common features (Kedrov et al., 2007; Oesterhelt et al., 2000). However, superimpositions do not allow force and probability to be determined. In addition, distances in F-D curves are given in metric units, making it difficult to correlate force peaks with portions of the stretched peptide. To directly correlate the force peaks to the stretched polypeptide lengths, we introduce a new procedure to analyze the F-D spectra. First, we fit every force peak detected in a single F-D curve using the WLC model (Muller et al., 2002). From each fit we obtain the length of the stretched polypeptide and the rupture force of each peak. Analyzing every F-D curve provides the probability and the average force at which a certain force peak is detected. Replacing the WLC fitted pulling distance with the polypeptide length allows mapping interaction force and probability onto the unfolded polypeptide (Figures 2 and 3). As noted previously, the average force includes only data from detected force peaks. To be able to determine the true average strength of interactions established within all NpSRII molecules, the average force had to be normalized. Therefore, we multiplied the peak probability and average force for every stretched length of the polypeptide (Figure 4A). This normalized average force presents the interaction strength that can be expected in a randomly picked NpSRII molecule, or in other words, the average interaction strength in NpSRII.

Interactions Occurring upon Transducer Binding Are Localized

The histograms shown in Figures 2 and 3 allow a coarse correlation of interactions measured for the stretched polypeptide

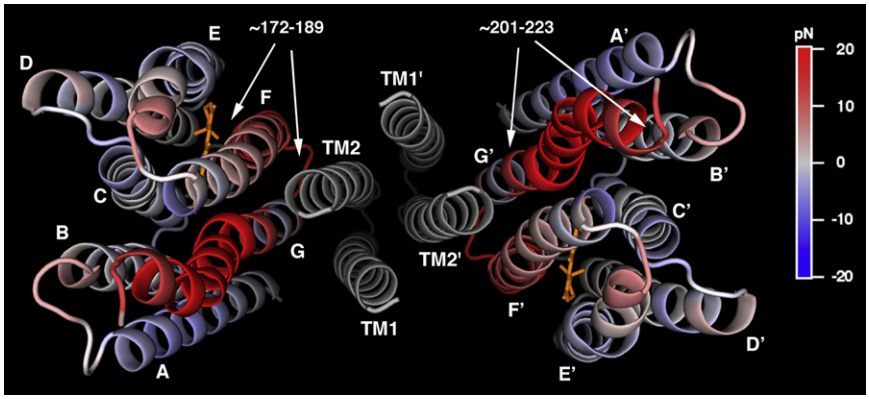

Figure 5. Structural Map of Interactions That Change upon NpHtrII$_{114}$ to NpSRII Binding

The X-ray structure of the NpSRII + NpHtrII$_{114}$ heterodimeric complex (Gordeliy et al., 2002) was color scaled to visualize changes in normalized average interaction forces. To visualize subtle changes in the interaction force, the color scale ranges from −20 to 20 pN (note that interaction forces detected at helix G can scale up to ~80 pN; see Figure 4B). Positive changes (red) indicate interactions strengths increasing upon NpHtrII$_{114}$ binding. Transmembrane α helices of NpSRII are named from A to G. Transmembrane α helices TM1 and TM2 belong to the truncated transducer (NpHtrII$_{114}$).

lengths to positions at which these interactions occur in the NpSRII polypeptide. After correcting the location of the interactions that are within the membrane bilayer or on the side of the membrane opposite to the pulling AFM tip (see Experimental Procedures), the peaks are more accurately mapped onto the NpSRII polypeptide (Figure 4). The map calculated by finding the difference between the normalized average interactions of NpSRII alone and of NpSRII in complex with the transducer (Figure 4A) locates the polypeptide regions at which intramolecular interactions changed upon transducer binding (Figure 4B). The predominant changes were at WLC fitted polypeptide lengths of ~34 aa and ~45 aa (Figure 4B, lower x axis of histogram), which correlate to amino acid positions ~211 and ~174 as counted from the N-terminal end (Figure 4B, upper x axis of histogram), respectively. These maxima locate to structural regions of transmembrane α helices F and G. Whereas transducer binding enhances the normalized interaction strength at transmembrane α helix G by ~80 pN, that established at α helix F is enhanced by only ~18 pN.

The force histograms (Figures 2 and 4A) show that the peaks at ~34 aa and ~45 aa were detected in NpSRII independent of the transducer binding. In the case of bacteriorhodopsin (Muller et al., 2002) and halorhodopsin (Cisneros et al., 2005), SMFS detects interactions at the same positions. Thus, interactions and locations appear to be conserved among all three archaeal rhodopsins. Upon transducer binding, both interactions are strengthened. This leads to several conclusions. First, transducer binding specifically influences certain interactions within the NpSRII molecule. Two transmembrane α helices, F and G, are affected, whereas the other five α helices show no changes in their interaction strengths. Second, the transducer binding does not alter the NpSRII molecule enough to establish interactions at new positions. Third, the magnitude of changes to the interactions introduced upon transducer binding at helices F and G scale differently (Figure 4). The strengthening at α helix G appears to be more than four times stronger then at α helix F, suggesting a tighter interaction with the transducer.

NpSRII Interactions in the Vicinity of Transducer Binding Are Strengthened

To visualize the location of interaction differences we mapped these onto the 3D structure of the NpSRII + NpHtrII complex (Figure 5). In good agreement, the regions most affected—α helices G and F—form the NpHtrII binding site (Gordeliy et al., 2002). Alpha helices F and G also shield the remaining helices, A–E, from direct interactions with the transducer. This may explain why we did not detect any changes to interactions in these structures, neither in probability (Figure 2) nor in force (Figure 3). This finding indicates the absence of long-range interactions (Sapra et al., 2008) introduced by the transducer and bridging to structures different from α helices F and G. Thus, we assume that α helices F and G interact with the transducer independently of the other NpSRII structural regions. This is consistent with the receptor structure being almost identical with and without transducer (Luecke et al., 2001; Gordeliy et al., 2002).

It may be argued that the structure of NpSRII relaxes after the first α helices have been unfolded by SMFS. Such a relaxation would disfavor detecting changes to the α helices remaining folded in the membrane. Though membrane proteins typically fold into a membrane bilayer in seconds, SMFS, as applied here, forces transmembrane helices to unfold in 10–20 microseconds. Although quick, the microsecond time range may allow small structural rearrangements within the folded part of the protein. Thus, it may be that SMFS does not probe the native structures within a membrane protein. Molecular dynamics (MD) simulations investigating the SMFS-induced unfolding process of bacteriorhodopsin indicate that membrane protein structures remain unchanged during the mechanical unfolding process (Cieplak et al., 2006; Seeber et al., 2006). However, these MD simulations were done at much faster pulling speed than experimentally used (Kedrov et al., 2007). Nevertheless, MD simulations and experiments suggest that unpulled structures of an unfolding membrane protein remain largely unchanged. Findings in accordance with this observation are provided by experiments on the H^+/Na^+ antiporter NhaA. While unfolding NhaA by SMFS, it was possible to observe the binding of a ligand to a transmembrane α helix residing in the middle of the structure (Kedrov et al., 2005). Furthermore, from the F-D data it was possible to distinguish whether a ligand or an inhibitor was bound to the antiporter (Kedrov et al., 2006, 2008). Independent of small rearrangements to structural elements that may occur while unfolding the protein, SMFS allows comparative measurements. Here we compared the interactions established in free NpSRII molecules with those in NpSRII bound to NpHtrII$_{114}$ and determined where and to which extent transducer binding induced changes to NpSRII. To what extent our comparative experiments reflect the absolute interaction strengths established within native proteins needs to be shown.

Binding of NpHtrII to NpSRII Helices F and G May Have Possible Functional Consequences

NpSRII function as a light-driven proton pump (Schmies et al., 2000, is suppressed by the binding of the transducer NpHtrII (Schmies et al., 2001). Proton transport has been thoroughly studied in the structurally and functionally related bacteriorhodopsin (Haupts et al., 1999; Oesterhelt and Stoeckenius, 1973; Subramaniam and Henderson, 2000). A key event is the opening of the proton channel on the cytoplasmic side of the membrane, which is accompanied by tilting transmembrane α helix F (Koch et al., 1991; Moukhametzianov et al., 2006; Yoshida et al., 2004). This conformational change provides the basis for reprotonation of the Schiff base. Binding of NpHtrII to NpSRII is aided by hydrogen bonds between Thr189 and Tyr199 of α helix G with transmembrane α helix TM2 of the transducer (Klare et al., 2004). Signal transduction is controlled by the receptor, in particular by Thr204 (α helix G) and its hydrogen-bonded partner Tyr174 (α helix F). These two residues are essential for phototaxis (Sudo et al., 2006), and their introduction into bacteriorhodopsin converts the proton pump to, like SRII, activate HtrII (Sudo and Spudich, 2006). This demonstrates the key role of residues and hosting α helices F and G.

In recent years, several biophysical techniques have been applied to investigate possible structural rearrangements occurring at the interface between receptor and transducer. The interactions between NpSRII and NpHtrII appear to couple the light-induced conformational change of α helix F to signal transduction (Wegener et al., 2000; Klare et al., 2004). FTIR, FRET, molecular dynamics simulations, and EPR spectroscopy yielded partly contradictory results on light-induced structural rearrangements of transmembrane α helices F and G of the receptor and α helix TM2 of the transducer (Bordignon et al., 2007). In absence of the transducer, α helix F bends outward, allowing uptake and pumping of the proton from the cytoplasmic side of the membrane. In the presence of the transducer, this proton pumping mechanism is impaired. FTIR measurements by the Spudich group suggested that the reconstituted NpSRII + $NpHtrII_{147}$ fusion complex undergoes conformational changes consistent with an outward tilting of α helix F (Bergo et al., 2003). In apparent contrast, FTIR measurements (Kamada et al., 2006) suggested that the opening of the cytoplasmic cleft required for the proton uptake does not occur in phosphatidylcholine reconstituted NpSRII in the presence of the transducer. However, EPR measurements of the NpSRII + $NpHtrII_{114}$ complex reconstituted into purple membrane lipids, such as investigated in our study, suggest that during receptor activation, α helix F undergoes conformational changes both in the presence and absence of the transducer (Bordignon et al., 2007; Wegener et al., 2000). Light-induced isomerization of the retinal is proposed to induce specific conformational changes to the receptor that triggers an outward motion of transmembrane α helix F. In this motion, α helix F slides along α helix G, whose structure remains unchanged, and induces a clockwise rotary motion of transmembrane α helix TM2 to activate the transducer. The evidence of a conformational change is contradicted by the X-ray structures of the inactivated and illuminated NpSRII + NpHtrII complex (Moukhametzianov et al., 2006). Here, the light-induced isomerization of the retinal does not cause conformational changes in α helix F. This finding is surprising because the transducer appears to be structurally altered in α helix TM2. It is assumed that the interactions with the transducer inhibit conformational changes of α helix F. However, loop EF of the receptor in the 3D crystal forms contacts with other proteins. Because the flexibility of the EF loop is important for the outward tilting of helix F (Koch et al., 1991; Subramaniam and Henderson, 2000), the crystal-specific contact of the EF loop may inhibit this motion.

Our SMFS measurements reveal that the binding of $NpHtrII_{114}$ to NpSRII significantly increases the interactions established at transmembrane α helices F and G (Figure 4B). Compared with transmembrane α helix F, α helix G exhibited an almost 4-fold higher increase of interactions strength. In α helix G these interactions induced by the transducer are distributed over nearly the entire helix, whereas α helix F is stabilized only at its extracellular end (Figure 5). Previously, in the case of the H^+/Na^+ antiporter NhaA, we showed that inhibitor binding enhances the interactions at transmembrane α helix IX and reduces its structural flexibility (Kedrov et al., 2006, 2008). Analogous to this finding, we speculate that the strengthening of the existing interactions at transmembrane α helix G of NpSRII further stabilizes this helix and reduces its flexibility. Similarly, transducer binding enhances the stability and thus may reduce the flexibility at the extracellular end of α helix F. Most importantly, both structural domains exhibiting significantly enhanced stability and reduced flexibility must act differently in NpSRII complexed with the transducer. The enhanced stability and reduced flexibility of helix G leads to the assumption that this structure will remain unchanged upon light-induced activation of the NpSRII + $NpHtrII_{114}$ complex. In contrast, the transducer binding "pins" α helix F only at its extracellular end. It may be that this pinning of the structure guides the cytoplasmic end of the helix to enable efficient signal transduction. Such a model is supposed by EPR measurements (Bordignon et al., 2007; Wegener et al., 2001) in which light activation of the receptor induces an outward motion of α helix F along G to activate the transducer. However, in our SMFS measurements we can only detect and locate interactions in NpSRII. Thus, interpretations of how such interactions may guide conformational changes of a receptor remain speculative until further insights are obtained. Our findings show how transducer binding changes the interactions and coupling within the receptor in a way that proton pumping is inhibited (Spudich, 1998) and signal transduction enabled.

Conclusion

Using SMFS, we detected interactions within NpSRII without and with its transducer bound. To reveal the differences between transducer bound and unbound states we introduced a simple way to analyze the F-D spectra. The analysis revealed the strength and structural location of intramolecular interactions within the average receptor. Binding of the transducer to NpSRII enhanced intramolecular interactions that already existed at transmembrane α helices G and F. We suggest that the specific binding of the transducer and its ability to strengthen key interactions at α helices F and G of NpSRII "prime" the receptor for signaling rather than ion pumping. This binding, with its specific interactions, may reflect a mechanism by which the receptor-transducer interaction could have evolved without compromising the photocycle of microbial rhodopsins.

EXPERIMENTAL PROCEDURES

Sample Preparation

NpSRII and NpHtrII$_{114}$ from *N. pharaonis* were overexpressed as His-tagged proteins in *Escherichia coli* and purified by affinity chromatography using a Ni-NTA agarose column (QIAGEN, Hilden, Germany). NpSRII was then reconstituted into purple membrane lipids with a 1:35 (w/w) protein-to-lipid ratio (Hohenfeld et al., 1999). NpSRII + NpHtrII$_{114}$ complexes were prepared by mixing NpSRII and NpHtrII$_{114}$ at a ratio of 1:1 followed by reconstitution into lipids (Wegener et al., 2001).

SMFS

SMFS on NpSRII and NpSRII + NpHtrII$_{114}$ complexes was performed as described (Muller et al., 2002; Oesterhelt et al., 2000). Membrane patches containing the reconstituted NpSRII were adsorbed to the mica support and visualized by AFM. After imaging, the AFM was switched to the SMFS mode. The AFM tip was then pushed onto the protein membrane until a terminal end of the protein adsorbed to the tip by unspecific interactions (Janovjak et al., 2003; Oesterhelt et al., 2000). The AFM tip was then retracted from the membrane surface at a velocity of ~300 nm/s. Force-versus-distance (F-D) curves were obtained by recording the cantilever deflection over the separation distance. Si_3N_4 cantilevers (model NP-S, nominal spring constant ~0.06 N/m and resonance frequency ~18 kHz; Veeco Instruments, Santa Barbara, CA) were used for imaging and force spectroscopy. All cantilevers showed a spring constant of ~0.07 ± 0.01 N/m, which was determined using the equipartition theorem (Butt et al., 1995).

As in previous studies, the length of F-D spectra was used to discard F-D curves that resulted from the attachment of the AFM tip with regions of the polypeptide other than the terminal ends (Cisneros et al., 2005; Muller et al., 2002). The N-terminal end of NpSRII forms a 1 or 2 aa-long end of α helix A, which is mainly embedded in the membrane (Luecke et al., 2001). Because of this limited exposure, the probability of the N-terminal end attaching to the AFM tip was assumed to be very low. The C-terminal end is longer (~23 aa) and, thus, has a much higher probability of attaching to the AFM tip. We assume that upon mechanically pulling from a terminal end all transmembrane α helices unfold sequentially from this end while the tip is separated from the membrane. The maximum length of the stretched polypeptide, indicated by the last force peak, measures the stability of the last α helix embedded in the membrane. Thus the maximum length of the stretched polypeptide can be estimated by the polypeptide stretch from the terminal end pulled to this last α helix (Kedrov et al., 2004; Kessler and Gaub, 2006). This simple model predicts different maximum lengths of F-D curves obtained for pulling at the N-terminal or C-terminal ends of NpSRII. Mechanical unfolding of the first six transmembrane α helices results in a stretched polypeptide segment of ~60 nm (~200 aa) length when pulling from the N-terminal end, and lengths ranging between 60 and 65 nm (202–219 aa) when pulled from the C-terminal end. Therefore, F-D curves obtained from pulling at either terminal end could be separated from each other. Thus, to analyze only F-D curves obtained pulling single NpSRII molecules from the C-terminal end, we selected curves exhibiting lengths ≥60 nm.

In contrast to this unambiguous criterion, the classification and analysis of shorter F-D curves was not attempted. For example, F-D curves of lengths between 50 and 60 nm represent NpSRII pulled from either the C- or the N-terminal end. Even shorter F-D curves may have resulted from picking the NpSRII molecule from one of its polypeptide loops. These F-D curves cannot be used because pulling at different loops results in F-D curves of similar lengths. In addition, protein and AFM tip frequently unbind during mechanically pulling, resulting in abortive short F-D curves. These considerations are further complicated by the presence of the transducer, which may be unfolded from either terminal end, resulting in F-D curves of similar lengths as expected when unfolding NpSRII from either its CD or EF loops. Therefore, we focused our data analysis on F-D curves that resulted from full unfolding and stretching of NpSRII by pulling at the C-terminal end.

After selecting a sufficiently long F-D curve (≥60 nm), each force peak was fitted using the wormlike chain (WLC) model (Bustamante et al., 1994). The contour length (L) of the stretched polypeptide was obtained from the WLC fit assuming a persistence length (l_p) of 0.4 nm (Oesterhelt et al., 2000). Equally, for each peak the rupture force was measured. To locate the interactions corresponding to force peaks onto the NpSRII structure (1H2S; Gordeliy et al., 2002), the contour length at which this peak occurred was subtracted from the C-terminal end.

When pulling the protein from the C-terminal end, the interaction anchoring the stretched polypeptide segment was sometimes not located at the cytoplasmic end of an α helix, but at the opposite N-terminal surface. In this case, the effective length of the stretched polypeptide was longer and the lipid membrane thickness (~4 nm) had to be considered. In this case, we added 11 aa (11 × 0.36 nm ≈ 4 nm) to the number of amino acids determined by the WLC model (Muller et al., 2002). If a segment was shorter than the width of the membrane, a fraction of the membrane thickness (11 aa) proportional to the length of the apparent stretched polypeptide was added. To visualize the interactions within NpSRII that have changed upon NpHtrII binding, the histograms of the normalized interaction forces measured for NpSRII with and without the transducer NpHtrII$_{114}$ (Figure 4A) were subtracted from each other. To avoid artifacts, the resulting histogram was smoothed by an algorithm that distributed 25% of the counts of each bin to the previous and following bin. The differences of the normalized forces were then mapped onto the NpSRII structure.

ACKNOWLEDGMENTS

This work was supported by the Deutsche Forschungsgemeinschaft (DFG), the European Union (FP6), and the Free State of Saxony. We thank Annika Göppner for excellent technical help, and Georg Büldt, Tanuj Sapra, and Daniel Silva for helpful discussions.

Received: February 17, 2008
Revised: April 11, 2008
Accepted: April 11, 2008
Published: August 5, 2008

REFERENCES

Bergo, V., Spudich, E.N., Spudich, J.L., and Rothschild, K.J. (2003). Conformational changes detected in a sensory rhodopsin II-transducer complex. J. Biol. Chem. *278*, 36556–36562.

Bordignon, E., Klare, J.P., Holterhues, J., Martell, S., Krasnaberski, A., Engelhard, M., and Steinhoff, H.J. (2007). Analysis of light-induced conformational changes of *Natronomonas pharaonis* sensory rhodopsin II by time resolved electron paramagnetic resonance spectroscopy. Photochem. Photobiol. *83*, 263–272.

Bustamante, C., Marko, J.F., Siggia, E.D., and Smith, S. (1994). Entropic elasticity of lambda-phage DNA. Science *265*, 1599–1600.

Butt, H.J., Jaschke, M., and Ducker, W. (1995). Measuring surface forces in aqueous electrolyte solution with the atomic force microscope. Bioelectrochem. Bioenerg. *38*, 191–201.

Chizhov, I., Schmies, G., Seidel, R., Sydor, J.R., Luttenberg, B., and Engelhard, M. (1998). The photophobic receptor from *Natronobacterium pharaonis*: temperature and pH dependencies of the photocycle of sensory rhodopsin II. Biophys. J. *75*, 999–1009.

Cieplak, M., Filipek, S., Janovjak, H., and Krzysko, K.A. (2006). Pulling single bacteriorhodopsin out of a membrane: comparison of simulation and experiment. Biochim. Biophys. Acta *1758*, 537–544.

Cisneros, D.A., Oesterhelt, D., and Muller, D.J. (2005). Probing origins of molecular interactions stabilizing the membrane proteins halorhodopsin and bacteriorhodopsin. Structure *13*, 235–242.

Gordeliy, V.I., Labahn, J., Moukhametzianov, R., Efremov, R., Granzin, J., Schlesinger, R., Buldt, G., Savopol, T., Scheidig, A.J., Klare, J.P., et al. (2002). Molecular basis of transmembrane signalling by sensory rhodopsin II-transducer complex. Nature *419*, 484–487.

Haupts, U., Tittor, J., and Oesterhelt, D. (1999). Closing in on bacteriorhodopsin: progress in understanding the molecule. Annu. Rev. Biophys. Biomol. Struct. *28*, 367–399.

Hohenfeld, I.P., Wegener, A.A., and Engelhard, M. (1999). Purification of histidine tagged bacteriorhodopsin, pharaonis halorhodopsin and pharaonis

sensory rhodopsin II functionally expressed in *Escherichia coli*. FEBS Lett. *442*, 198–202.

Janovjak, H., Kessler, M., Oesterhelt, D., Gaub, H., and Muller, D.J. (2003). Unfolding pathways of native bacteriorhodopsin depend on temperature. EMBO J. *22*, 5220–5229.

Janovjak, H., Kedrov, A., Cisneros, D.A., Sapra, K.T., Struckmeier, J., and Muller, D.J. (2006). Imaging and detecting molecular interactions of single transmembrane proteins. Neurobiol. Aging *27*, 546–561.

Kamada, K., Furutani, Y., Sudo, Y., Kamo, N., and Kandori, H. (2006). Temperature-dependent interactions between photoactivated pharaonis phoborhodopsin and its transducer. Biochemistry *45*, 4859–4866.

Kedrov, A., Ziegler, C., Janovjak, H., Kuhlbrandt, W., and Muller, D.J. (2004). Controlled unfolding and refolding of a single sodium-proton antiporter using atomic force microscopy. J. Mol. Biol. *340*, 1143–1152.

Kedrov, A., Krieg, M., Ziegler, C., Kuhlbrandt, W., and Muller, D.J. (2005). Locating ligand binding and activation of a single antiporter. EMBO Rep. *6*, 668–674.

Kedrov, A., Ziegler, C., and Muller, D.J. (2006). Differentiating ligand and inhibitor interactions of a single antiporter. J. Mol. Biol. *362*, 925–932.

Kedrov, A., Janovjak, H., Sapra, K.T., and Muller, D.J. (2007). Deciphering molecular interactions of native membrane proteins by single-molecule force spectroscopy. Annu. Rev. Biophys. Biomol. Struct. *36*, 233–260.

Kedrov, A., Appel, M., Baumann, H., Ziegler, C., and Muller, D.J. (2008). Examining the dynamic energy landscape of an antiporter upon inhibitor binding. J. Mol. Biol. *375*, 1258–1266.

Kessler, M., and Gaub, H.E. (2006). Unfolding barriers in bacteriorhodopsin probed from the cytoplasmic and the extracellular side by AFM. Structure *14*, 521–527.

Klare, J.P., Gordeliy, V.I., Labahn, J., Buldt, G., Steinhoff, H.J., and Engelhard, M. (2004). The archaeal sensory rhodopsin II/transducer complex: a model for transmembrane signal transfer. FEBS Lett. *564*, 219–224.

Klare, J.P., Chizhov, I., and Engelhard, M. (2008). Microbial rhodopsins: scaffolds for ion pumps, channels, and sensors. Results Probl. Cell Differ. *45*, 73–122.

Klyszejko, A.L., Shastri, S., Mari, S.A., Grubmuller, H., Muller, D.J., and Glaubitz, C. (2008). Folding and assembly of proteorhodopsin. J. Mol. Biol. *376*, 35–41.

Koch, M.H.J., Dencher, N.A., Oesterhelt, D., Plöhn, H.-J., Rapp, G., and Büldt, G. (1991). Time-resolved X-ray diffraction study of structural changes associated with the photocycle of bacteriorhodopsin. EMBO J. *10*, 521–526.

Luecke, H., Schobert, B., Lanyi, J.K., Spudich, E.N., and Spudich, J.L. (2001). Crystal structure of sensory rhodopsin II at 2.4 Angstroms: insights into color tuning and transducer interaction. Science *293*, 1499–1503.

Moukhametzianov, R., Klare, J.P., Efremov, R., Baeken, C., Goppner, A., Labahn, J., Engelhard, M., Buldt, G., and Gordeliy, V.I. (2006). Development of the signal in sensory rhodopsin and its transfer to the cognate transducer. Nature *440*, 115–119.

Muller, D.J., Amrein, M., and Engel, A. (1997). Adsorption of biological molecules to a solid support for scanning probe microscopy. J. Struct. Biol. *119*, 172–188.

Muller, D.J., Kessler, M., Oesterhelt, F., Moller, C., Oesterhelt, D., and Gaub, H. (2002). Stability of bacteriorhodopsin α-helices and loops analyzed by single-molecule force spectroscopy. Biophys. J. *83*, 3578–3588.

Oesterhelt, D., and Stoeckenius, W. (1973). Functions of a new photoreceptor membrane. Proc. Natl. Acad. Sci. U.S.A. *70*, 2853–2857.

Oesterhelt, F., Oesterhelt, D., Pfeiffer, M., Engel, A., Gaub, H.E., and Muller, D.J. (2000). Unfolding pathways of individual bacteriorhodopsins. Science *288*, 143–146.

Park, P.S., Sapra, K.T., Kolinski, M., Filipek, S., Palczewski, K., and Muller, D.J. (2007). Stabilizing effect of Zn^{2+} in native bovine rhodopsin. J. Biol. Chem. *282*, 11377–11385.

Sapra, K.T., Besir, H., Oesterhelt, D., and Muller, D.J. (2006a). Characterizing molecular interactions in different bacteriorhodopsin assemblies by single-molecule force spectroscopy. J. Mol. Biol. *355*, 640–650.

Sapra, K.T., Park, P.S., Filipek, S., Engel, A., Muller, D.J., and Palczewski, K. (2006b). Detecting molecular interactions that stabilize native bovine rhodopsin. J. Mol. Biol. *358*, 255–269.

Sapra, K.T., Balasubramanian, G.P., Labudde, D., Bowie, J.U., and Muller, D.J. (2008). Point mutations in membrane proteins reshape energy landscape and populate different unfolding pathways. J. Mol. Biol. *376*, 1076–1090.

Schmies, G., Luttenberg, B., Chizhov, I., Engelhard, M., Becker, A., and Bamberg, E. (2000). Sensory rhodopsin II from the haloalkaliphilic *Natronobacterium pharaonis*: light-activated proton transfer reactions. Biophys. J. *78*, 967–976.

Schmies, G., Engelhard, M., Wood, P.G., Nagel, G., and Bamberg, E. (2001). Electrophysiological characterization of specific interactions between bacterial sensory rhodopsins and their transducers. Proc. Natl. Acad. Sci. U.S.A. *98*, 1555–1559.

Seeber, M., Fanelli, F., Paci, E., and Caflisch, A. (2006). Sequential unfolding of individual helices of bacterioopsin observed in molecular dynamics simulations of extraction from the purple membrane. Biophys. J. *91*, 3276–3284.

Sharma, A.K., Spudich, J.L., and Doolittle, W.F. (2006). Microbial rhodopsins: functional versatility and genetic mobility. Trends Microbiol. *14*, 463–469.

Spudich, J.L. (1998). Variations on a molecular switch: transport and sensory signalling by archaeal rhodopsins. Mol. Microbiol. *28*, 1051–1058.

Spudich, J.L. (2006). The multitalented microbial sensory rhodopsins. Trends Microbiol. *14*, 480–487.

Spudich, J.L., and Bogomolni, R.A. (1984). Mechanism of colour discrimination by a bacterial sensory rhodopsin. Nature *312*, 509–513.

Subramaniam, S., and Henderson, R. (2000). Molecular mechanism of vectorial proton translocation by bacteriorhodopsin. Nature *406*, 653–657.

Sudo, Y., and Spudich, J.L. (2006). Three strategically placed hydrogen-bonding residues convert a proton pump into a sensory receptor. Proc. Natl. Acad. Sci. U.S.A. *103*, 16129–16134.

Sudo, Y., Furutani, Y., Kandori, H., and Spudich, J.L. (2006). Functional importance of the interhelical hydrogen bond between Thr204 and Tyr174 of sensory rhodopsin II and its alteration during the signaling process. J. Biol. Chem. *281*, 34239–34245.

Wegener, A.A., Chizhov, I., Engelhard, M., and Steinhoff, H.J. (2000). Time-resolved detection of transient movement of helix F in spin-labelled *pharaonis* sensory rhodopsin II. J. Mol. Biol. *301*, 881–891.

Wegener, A.A., Klare, J.P., Engelhard, M., and Steinhoff, H.J. (2001). Structural insights into the early steps of receptor-transducer signal transfer in archaeal phototaxis. EMBO J. *20*, 5312–5319.

Yan, B., Takahashi, T., Johnson, R., and Spudich, J.L. (1991). Identification of signaling states of a sensory receptor by modulation of lifetimes of stimulus-induced conformations: the case of sensory rhodopsin II. Biochemistry *30*, 10686–10692.

Yoshida, H., Sudo, Y., Shimono, K., Iwamoto, M., and Kamo, N. (2004). Transient movement of helix F revealed by photo-induced inactivation by reaction of a bulky SH-reagent to cysteine-introduced pharaonis phoborhodopsin (sensory rhodopsin II). Photochem. Photobiol. Sci. *3*, 537–542.